COBISS: 1.01, DOI: 10.3986/ac.v51i2.10589

MICRO-KARSTIFICATION IN A STALAGMITE FROM KÜPELI CAVE, SOUTHERN TURKEY

MIKRO-KOROZIJA STALAGMITA V JAMI KÜPELI, JUŽNA TURČIJA

Muhsin EREN[1*], Muhammetmyrat PALVANOV[1], Selahattin KADİR[2] & Selim KAPUR[3]

Abstract UDC 551.435.843:552.2(560)

Muhsin Eren, Muhammetmyrat Palvanov, Selahattin Kadir & Selim Kapur: Micro-karstification in a stalagmite from Küpeli Cave, southern Turkey

This article deals with micro-karstification forming abundant dissolution features in a stalagmite from Küpeli Cave in southern Turkey. Dissolution occurs when cave water enriched with CO_2 from the soil and epikarst, and in certain conditions also from the cave atmosphere, seeps into the stalagmite. Here, we hypothesise that water is transmitted from the former surface of the stalagmite to the interior by the roughly vertical or diagonal notch-shaped pores formed by the enlargement of intercrystalline pores by dissolution. These slightly elongated pores randomly developed in the stalagmite under repeated conditions at different stages of the stalagmite formation, affecting the last few macroscopic growth layers (lamina set under the microscope) from its former surface, finally its upper end was covered by a newly forming growth layer. Later, when this water reaches the relatively more permeable growth layer surfaces, it flows along these surfaces, and diffuse dissolution features form. The dissolution features include micro-scale pitted and etched surface structures, rounded and enlarged crystal boundaries and intercrystalline pores, and the breakdown of relatively large crystals (≥ 4 μm) into nm sized smaller crystal aggregates. In the dissolution pores, calcite re-precipitation occurs as rim and pore-filling cements when the percolation water is sufficiently saturated with calcium carbonate in the stalagmite. Under the repeated conditions, the dissolution was followed by calcite re-precipitation in the stalagmite, probably due to seasonal variation in CO_2 and $CaCO_3$ contents of the water in the epikarst zone as well as within the stalagmite.

Keywords: Cave, speleothem, stalagmite, micro karstification, dissolution, mineralogy.

Izvleček UDK 551.435.843:552.2(560)

Muhsin Eren, Muhammetmyrat Palvanov, Selahattin Kadir & Selim Kapur: Mikro-korozija stalagmita v jami Küpeli, južna Turčija

V članku obravnavamo mikro-korozijske oblike v stalagmitu iz jame Küpeli v južni Turčiji. Korozijo kapnikov lahko povzroča prenikla voda, ki se v tleh, epikrasu ali jamski atmosferi obogati s CO_2 in pronica v kapnik. V članku postavimo domnevo, da je voda iz nekdanje površine stalagmita prodrla v notranjost vzdolž vertikalnih in diagonalnih por zarezne oblike, ki so nastale s korozivnim širjenjem medkristalnih por. Te podolgovate pore so precej naključno nastajale ob cikličnih pogojih rasti stalagmita in segajo nekaj rastnih plasti globoko pod površino stalagmita, ki jo je kasneje prekrila nova plast sige. Voda je ob pronicanju vzdolž teh por dosegla relativno bolj prepustno rastno ploskev in korodirala vzdolž le-te. Pri tem so nastale različne mikro-korozijske oblike, kot so korozijske jamice, zaobljene in povečane kristalne meje, medkristalne pore in nanometrski kristalni skupki, ki so nastali ob porušitvi večjih kristalov ((≥ 4 μm). V korozijskih porah se je kasneje na nekaterih mestih iz prenasičene vode ponovno izločal kalcit, bodisi zgolj na robovih por bodisi kot polnilo por. V cikličnih pogojih rasti je izločanje praviloma sledilo raztapljanju, verjetno zaradi sezonske spremenljivosti dostopnega CO_2 in v vodi raztopljenega kalcita.

Ključne besede: jama, siga, stalagmit, mikro-korozija.

[1] Department of Geological Engineering, Mersin University, TR-33343, Çiftlikköy, Mersin, Turkey, e-mails m_eren@yahoo.com, fizikmuha93@gmail.com
[2] Department of Geological Engineering, Eskişehir Osmangazi University, TR-26480, Meşelik, Eskişehir, Turkey, e-mail: skadir.icc@gmail.com
[3] Department of Soil Science and Plant Nutrition, Çukurova University, TR-01330, Balcalı, Adana, Turkey, e-mail: kapurs@cu.edu.tr
* Corresponding author

Prejeto/Received: 24. 1. 2022

1. INTRODUCTION

Speleothems are cave deposits that mainly precipitate as calcite and aragonite from calcium carbonate ($CaCO_3$) rich percolating waters (Onac & Forti, 2011). The most common types of speleothems are stalagmites, stalactites, and flowstones. Stalagmite is used to describe a form of speleothem formation that grows upwards beneath dripping water on the cave floor (Frisia, 2019). Their longitudinal sections show well-developed macroscopic to microscopic size lamination, often represented by light and dark coloured alternating laminae due to seasonal growths (Aharon et al., 2006). These laminae are usually thick in the central part of stalagmites and get thinner towards the flanks. The majority of the studies on stalagmites have been conducted on stable isotope compositions due to their significance in the paleoclimatic reconstruction (e.g., Bar-Matthews et al., 1997; Vaks et

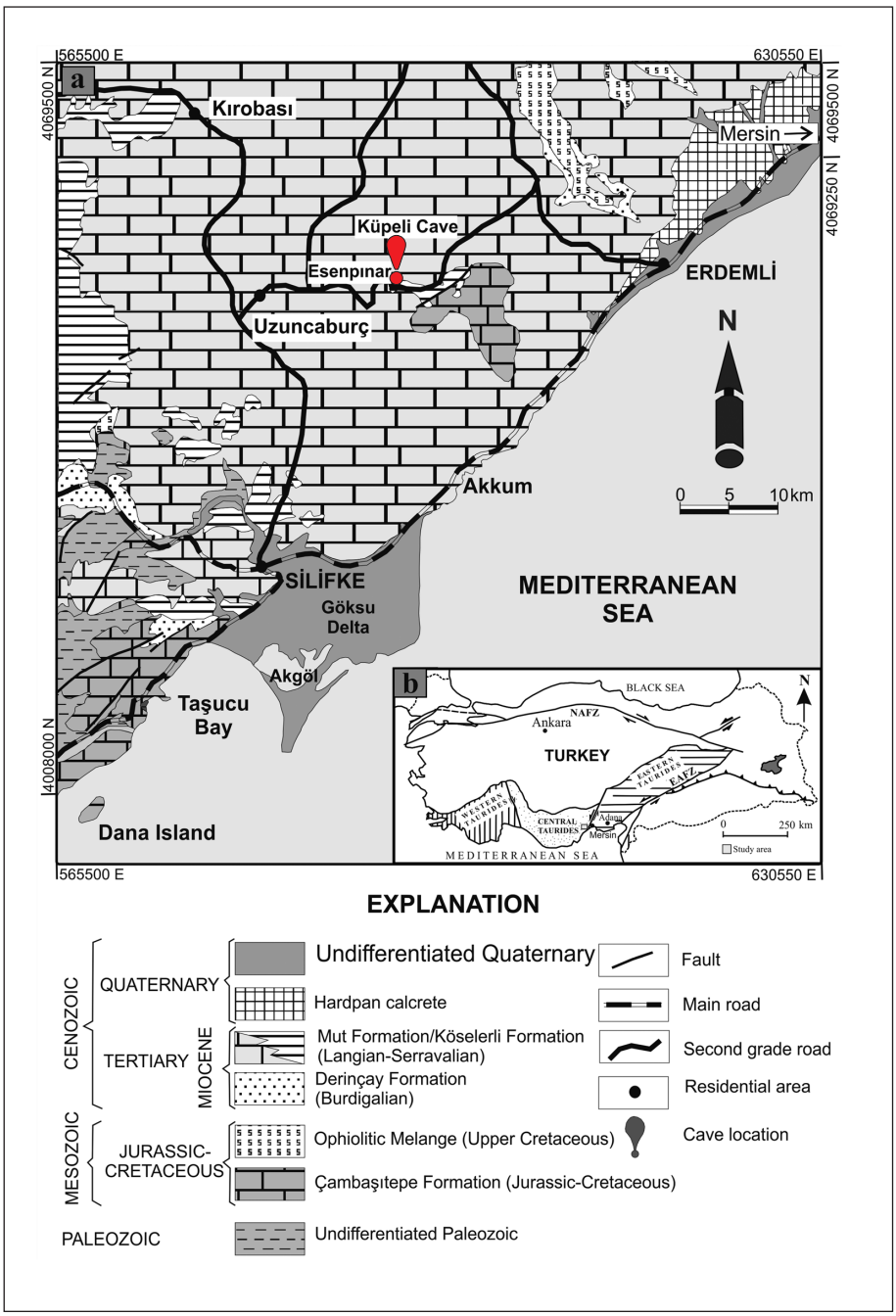

Figure 1: a) Geological map of the study area where Küpeli Cave is marked in red (Eren, 2008); b) The map of Turkey showing the Tauride Orogenic Belt and its subdivisions (Özgül, 1983).

al., 2003; Domínguez-Villar et al., 2008; Verheyden et al., 2008; Ünal-İmer et al., 2016). Despite the abundance of paleoclimatic studies, early diagenetic modifications of the speleothems including dissolution have received little attention, only a few providing brief information on dissolution (Martín-García et al., 2009; Railsback et al., 2013; Perrin et al., 2014; Scholz et al., 2014; Shtober-Zisu et al., 2014). Despite receiving little attention, Kukuljan et al. (2021) emphasized the importance of dissolution and precipitation processes in karst areas for the global carbon cycle and paleoclimate reconstruction. Therefore, this study deals with microscale karstification in the selected stalagmite by describing the microscale dissolution properties and discusses their formation.

2. CAVE SETTING

Küpeli Cave is located ~1.7 km northeast of Esenpınar (Erdemli, Mersin) which is a small town in southern Turkey (Figure 1a). The cave entrance has a latitude of 599726 E and a longitude of 4051941 N (UTM: 36.606085 °N, 34.114917 °E), and an elevation of 742 meters a.s.l. The cave is located within the central part of the Tauride orogenic belt where platform carbonates are common (Figure 1b). Küpeli Cave was developed within the reefal limestone of the Mut Formation (Langian-Serravalian) characterized by the abundance of red algae and corals (Figures 1a, 2; Gedik et al., 1979; Eren, 2008). A Mediterranean-type semi-arid climate prevails in the region, having the mean annual values of precipitation (550 mm), evaporation (1296 mm), and temperature (18.7 °C) obtained from the meteorological measurements of 70-years [Turkish State Meteorological Service (DMI), 2020].

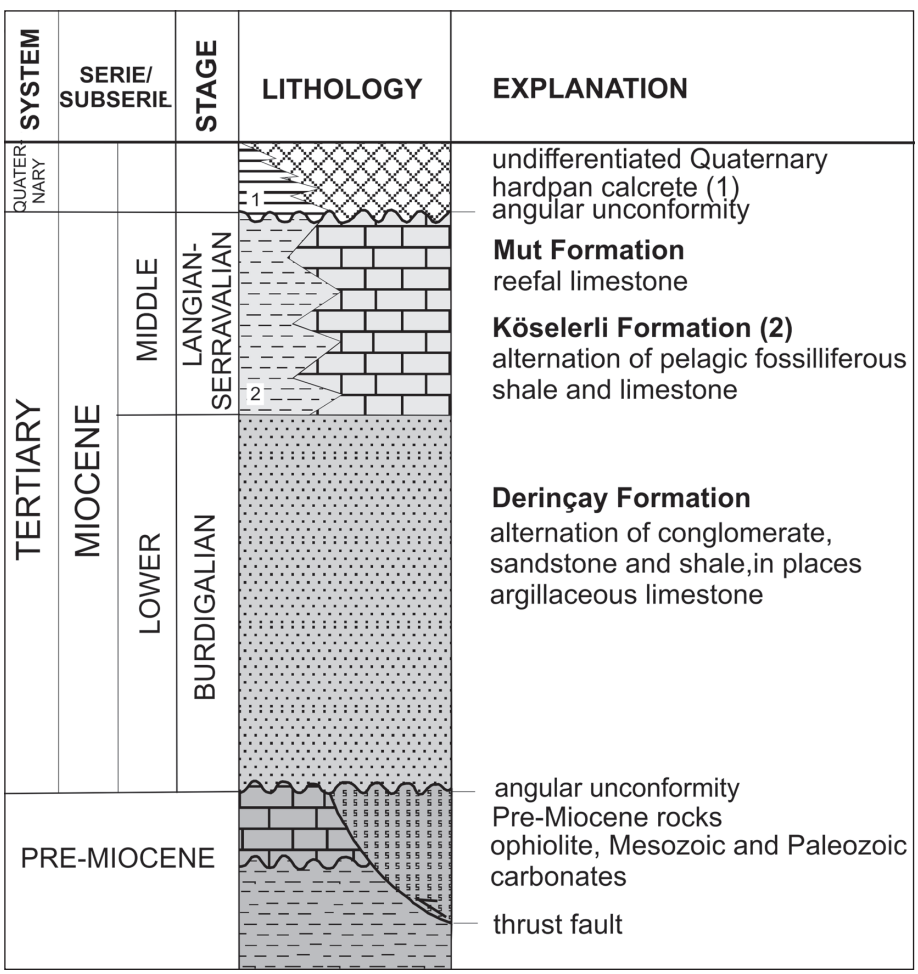

Figure 2: Generalized stratigraphical column of the study area (Eren, 2008).

3. CAVE DESCRIPTION

Küpeli Cave contains two chambers that are connected with each other with a narrow passage (Figure 3). The first chamber is 30 m long, 20 m wide, and 0.4 to 28 m in height. The entrance to the first chamber is provided by stairs from the collapsed portion of the roof. Whereas, the second chamber is of a smaller size being 17 m long, 9 m wide, and 38 m in height. The estimated thickness is 30-50 cm for soil cover and 6 to 10 m for epikarst zone above the cave.

The first room is well ventilated due to the collapse of the ceiling, yet the humidity is high but low compared to the second room. In the first room, small sized stalagmites with milky white tops and wet outer surfaces are common and may be indicative of actively occurring stalagmites. Earlier studies stated that the stalagmites of Turkey have formed at a time interval spanning from the Late Pleistocene to the Holocene (Fleitmann et al., 2009; Göktürk et al., 2011; Rowe et al., 2012; Ünal-İmer et al., 2015, 2016; Akgöz & Eren, 2015).

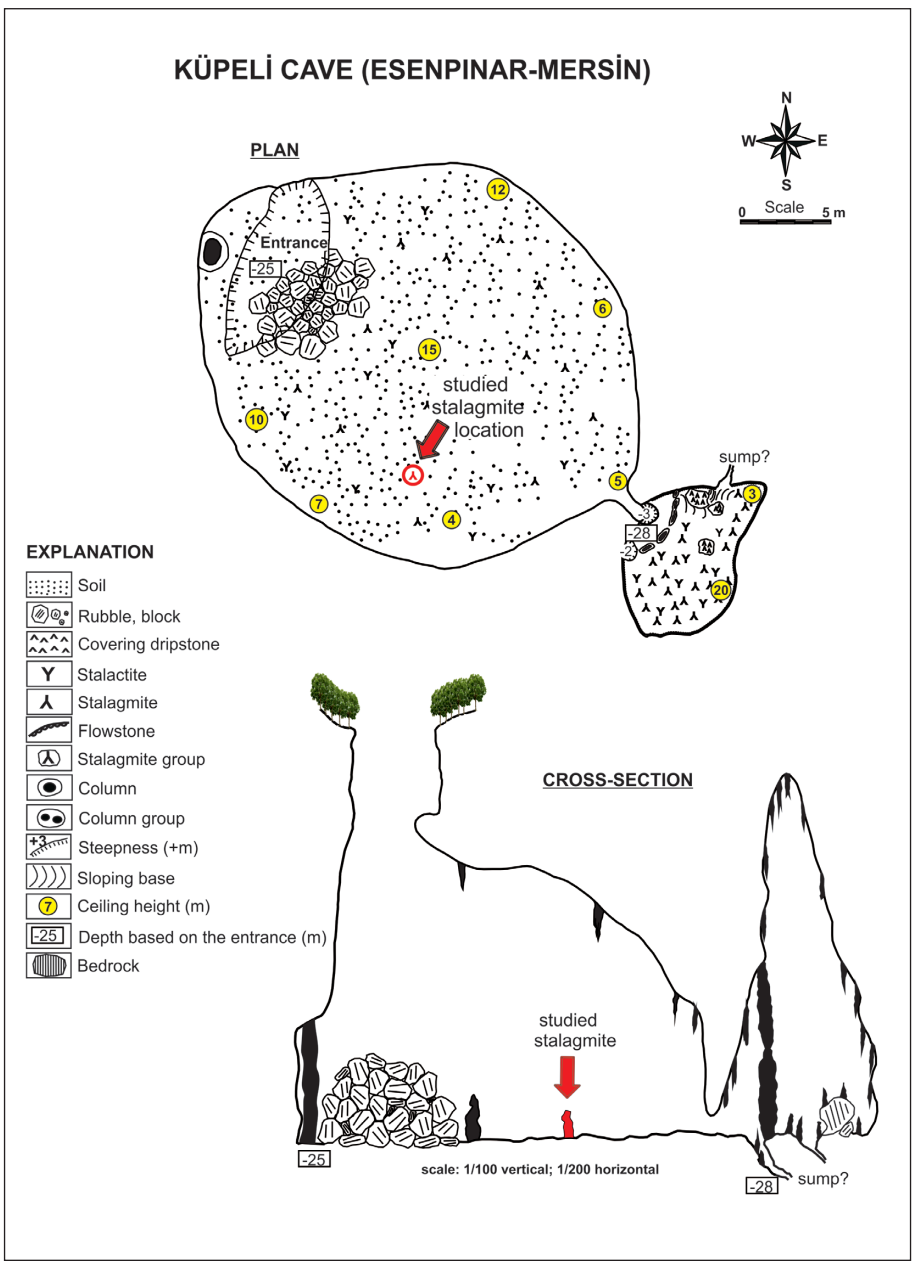

Figure 3: Plan view and vertical section of Küpeli Cave (modified from Akgöz, 2012).

4. MATERIAL AND METHODS

Several stalagmite samples were taken from the first chamber of Küpeli Cave to describe them and investigate their formation. A typical stalagmite was chosen in order to examine its micro-karstification features. The sample was divided into two parts by cross-cutting. Six thin sections were made from the surface of a longitudinal cross-section covering the entire surface and examined under a polarized microscope. Mineralogical compositions of the four bulk subsamples taken from the cross-sectional surface were determined by XRD using a Rigaku D / Max – 2200 Ultia PC with CuKα radiation and a scanning speed of 1°2θ min^{-1} at the General Directorate of Mineral Research and Exploration (MTA, Ankara, Turkey). The scanning electron microscopy and energy dispersive X-ray analyses (SEM–EDX) were performed on the six subsamples with size of ~6-7 mm at the Eskişehir Osmangazi University (Turkey), using using a Hitachi-Regulus 8230 FE–SEM instrument (Hitachi High-Tech, Tokyo, Japan) and an ULTIM EXTREME detector (Oxford Instruments, Abingdon, UK). The speleothem subsamples were prepared by adhering the freshly broken surfaces as well as dissolved elongated pore surface of the samples onto an aluminum sample holder with double-sided tape. The samples were then coated with a thin film (~3 nm) of gold/palladium using a Leica EM ACE600 (Leica Microsystems, Wetzlar, Germany).

5. RESULTS

5.1. STALAGMITE DESCRIPTION AND PETROGRAPHY

The studied stalagmite is in a wide cone shape with relatively flat top, which is associated with a small depresion (Figure 4a). The stalagmite is 12.5 cm high and 12.2 cm in diameter. Its vertical section along the growth axis exhibits well-developed macroscopic to microscopic size lamination (Figure 4b-c). The dark and light coloured alternating growth bands are usually thick (up to 1 cm) in the central part and thinner towards the stalagmite

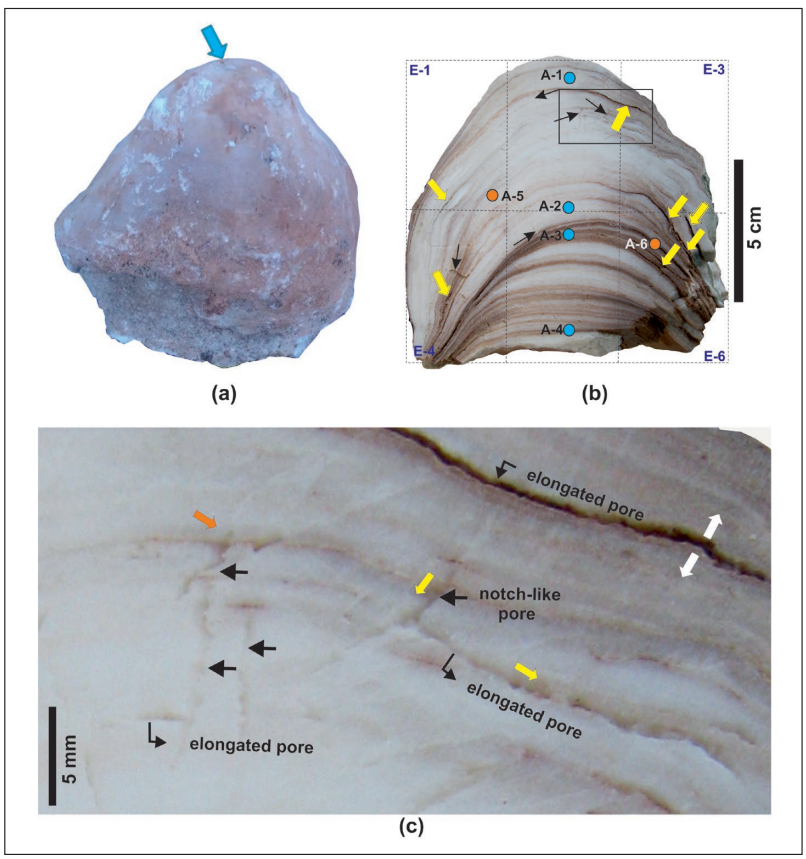

Figure 4: a) The stalagmite in a wide cone shape with a relatively flat top where a small depression is present (blue arrow); b) the vertical section along the growth axis of the stalagmite shows subvertical notch-like pores (black arrows) and elongated pores (yellow arrows) along the growth surface; c) close-up view of the frame in (b) showing notch-like pores (black arrows) cross-cutting one or more macroscopic growth layers and covered by the younger growth layer (orange arrow). The elongated pores extending along the growth layer surface. Yellow arrows show possible movement of leaking solvent water while white arrows indicate the easily concave/convex breakage surface of the stalagmite. E: thin section location, blue circle: subsample location with XRD and SEM analysis, orange circles: subsample location with SEM analysis.

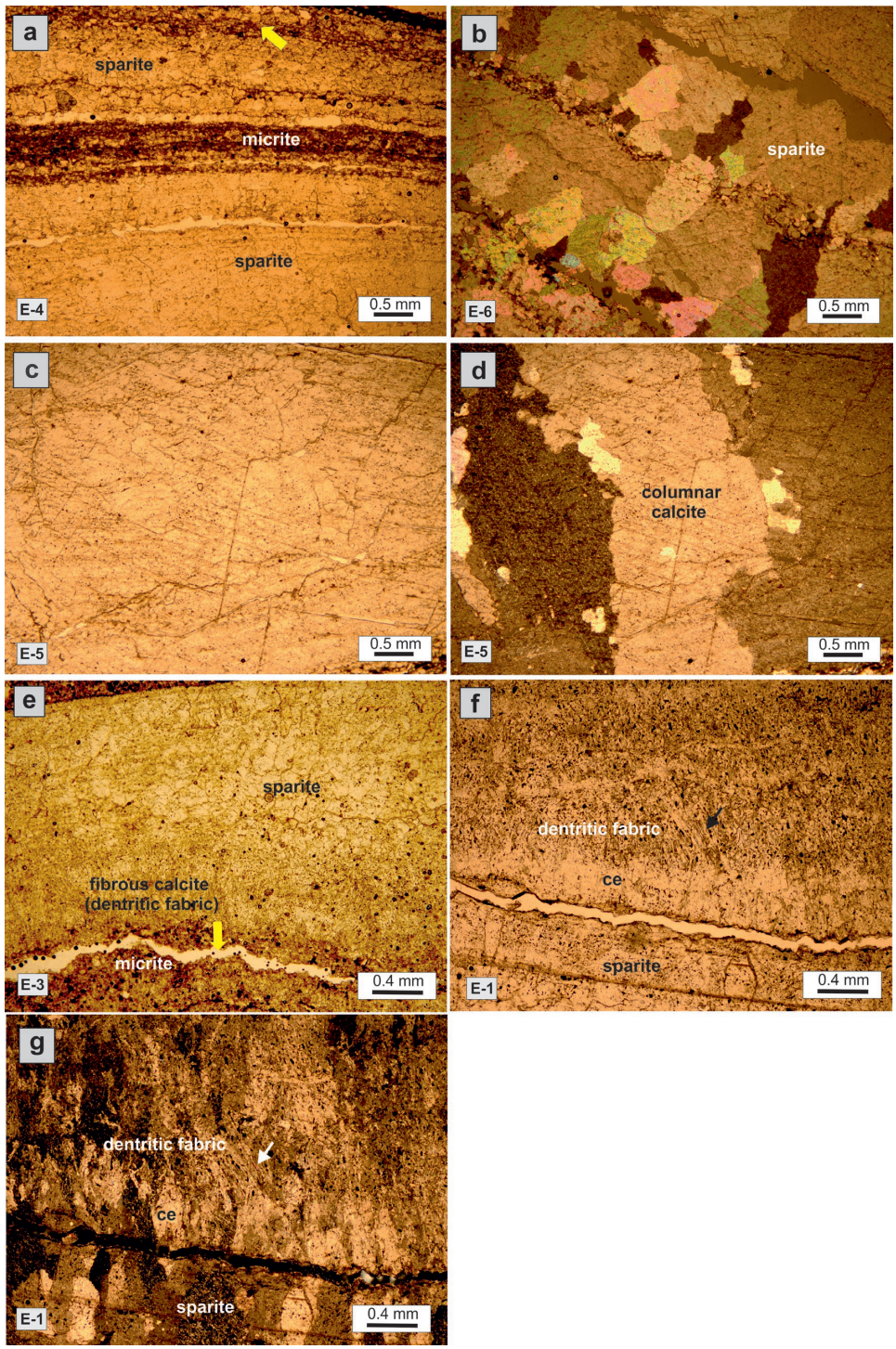

Figure 5: Micro-fabrics of the stalagmite: a) an alternation of sparitic and micritic (dark brown) growth layers under plane light. Recrystallization is common in micritic layers showing partial conversion to sparite (yellow arrow); b) sparite consisting of subhedral to euhedral crystals of calcite under cross-polarized light; c-d) columnar crystal fabric showing elongated calcite crystals under plane light (c) and cross-polarized light (d); e) a sequence of growth layers composed of micrite (partially recrystalized to sparite), dendritic fiber calcite and sparite under plane light; f-g) a dendritic fabric showing bundles of fiber calcite crystals (arrow) oriented at different directions under plane and cross-polarized light, respectively. ce: poikilotopic calcite cement engulfing the many fiber calcite crystals. Below the pore, there is a sparitic growth layer. E with a number indicates the thin section location on the cutting surface in Figure 4b.

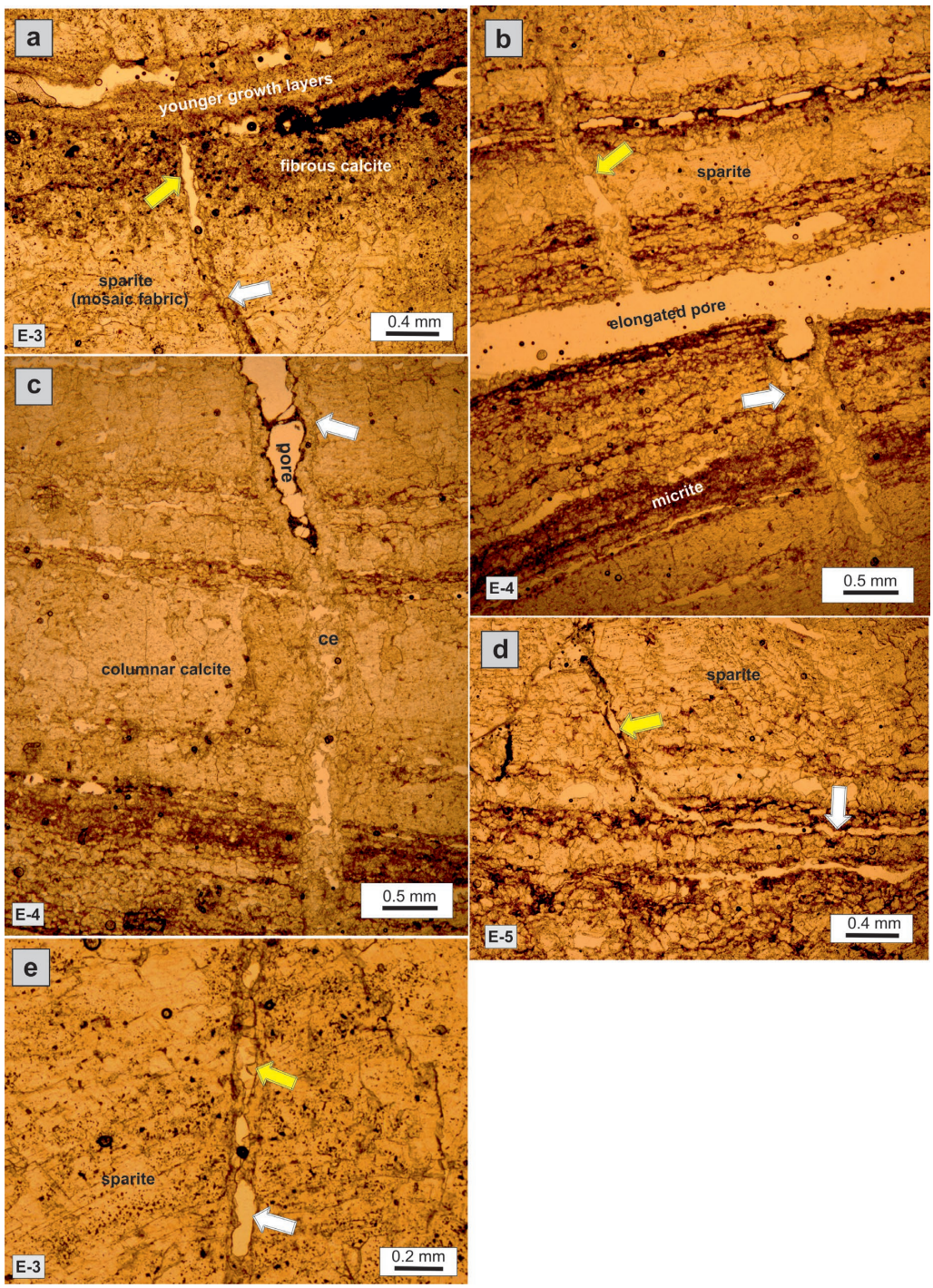

Figure 6: Microphotographs of the notch-like pores: a) subvertical notch-like pore (arrows) cross-cutting the growth layers often sparite with mosaic fabric and covered by younger growth layers. The upper part of the pore is empty (yellow arrow), formed by enlargement of intercrystalline pores whereas the lower part preserves its original fabric (white arrow) but acts a pathway for the water leakage; b) the vertical pore cross-cutting the growth layers shows two-part formation: the upper part (yellow arrow) transferred water to the elongated pores, then water found a new path for downward movement (white arrow); c) the vertical pore cross-cutting the layers, partially cemented by rim (white arrow) and pore-filling (ce) cements; d) the diagonal notch-like pore was converted to the elongated pore formed by enlargement of intercrystalline pores by dissolution; e) dog tooth cement in the notch-shaped pore formed by the dissolution of the intercrystalline pores in the sparite. All photomicrographs are under plane light and E with number shows thin-section location in Figure 4.

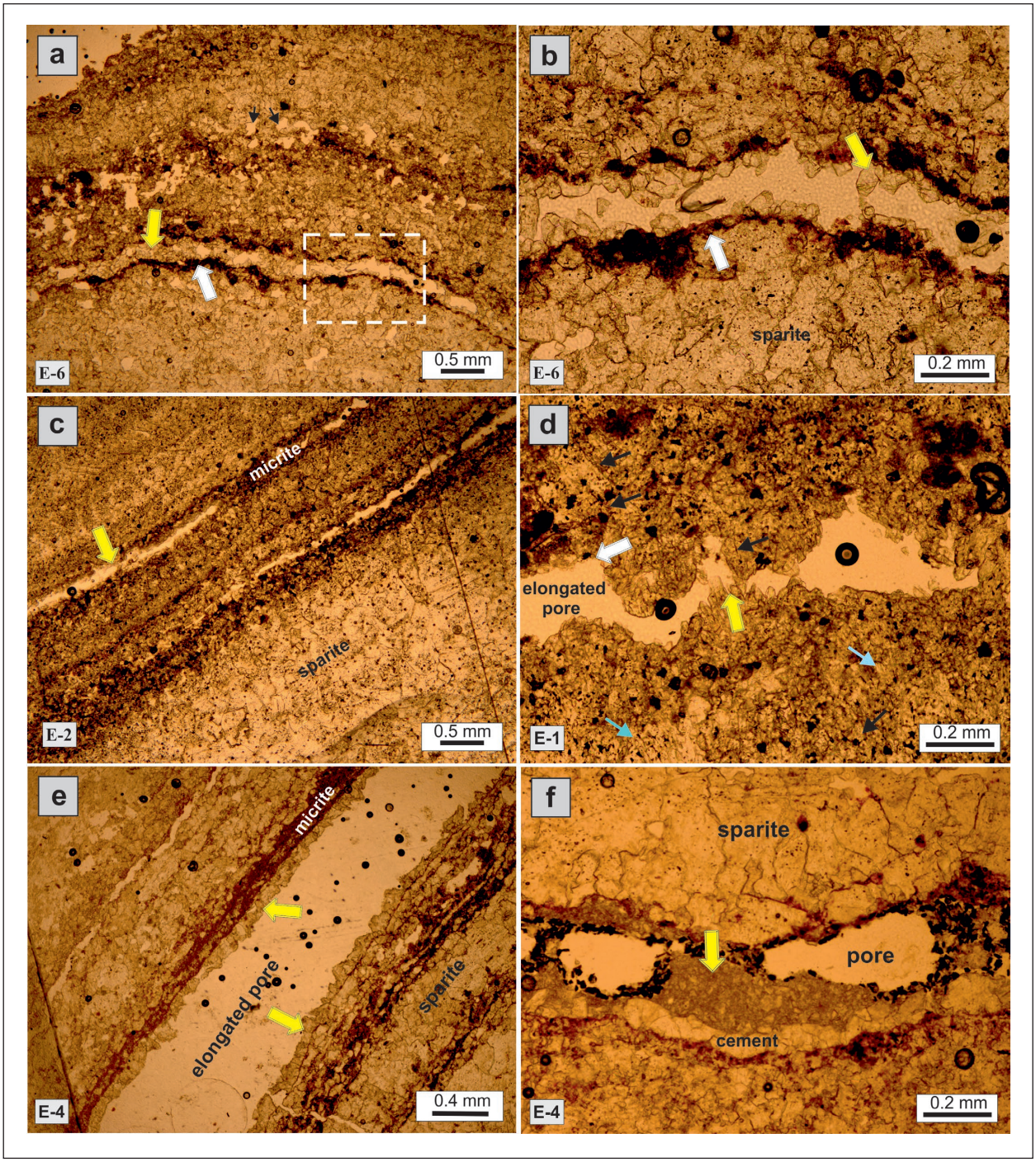

Figure 7: Microphotographs of the elogated pores developed along the growth layers: a) the elongated pore formed by dissolution throughout the growth layer, showing pore-filling cement (yellow arrow) as well as dog-tooth rim cement in the frame. The white arrow indicates the remnant of the primary micrite forming the growth layer; b) close up of the frame in (a) showing dog-tooth rim cement (yellow arrow) and pore surface with small irregularities (white arrow); c) the elongated pore partially developed within the micrite growth layer; d) the elongated pore within dentritic fabric that consists of cemented fiber calcite crystals (blue arrows). The pore shows dissolutional surface irregularities (white arrow) and dog-tooth rim cement (yellow arrow); e) the elongated pore with sparitic rim cement (yellow arrows); f) internal sediment (yellow arrow) in the elongated pore, consisting of clastic micrite and silt-sized carbonate grains on the cement. All photomicrographs are under plane light and E with number shows thin-section location in Figure 4.

flanks. Dark growth layers are more abundant in the lower part than the upper part. The cross-cut shows two main types of voids: notch-like (~1-2% of the total volume) and elongated (~5-7% of the total volume) (Figure 4b-c). They are observed inside the stalagmite, but not on the outer surface. The notch-like pores have a length of 1 cm and a width of ≤ 0.1 mm, cross-cut one to few macroscopic-sized growth layers below the former stalagmite surface, and their upper ends are covered by the younger growth layers (Figure 4c). Whereas the elongated pores are several cm in length and less than 0.4 mm in width and extend along the growth layer (Figure 4b-c).

Examination of the thin sections under the microscope reveals that the successive laminae show four common calcite microfabrics: mosaic, micrite, columnar, and dendritic (Figure 5). Mosaic microfabric consists of euhedral and roughly equant sparitic calcite crystals with sizes ranging from 0.6 to 1.2 mm (Figure 5b). The micrite layers are composed of micrite-sized calcite crystals (≤ 4 μm) appearing dark in colours, and were generally transformed into sparite after recrystallization (Figure 5a). The columnar microfabric is composed of elongated calcite crystals with variable sizes which are sub-parallel to the growth axis (Figure 5c-d). The dendritic micro-fabric is represented by the bundles or fans of fibrous crystals oriented at the two directions that extend roughly parallel to the growth axis and are up to1.0 mm long and 10-20 μm wide in size (Figure 5e-g).

Under the microscope, there are two main types of pores as mentioned above; notch-like and elongated (Figures 6, 7). The elongated pores are more abundant than the notch-like pores. The notch-like pores are approximately vertical or diagonal, intersecting the growth layers (Figure 6a-d). Despite to its sub-vertical cross cutting, they are more abundant in relatively thick sparitic layers under the microscope (Figure 6). Their upper end on the former stalagmite surface is covered by the young growth layers (Figure 6a). They are often associated with elongated pores (Figure 6b, d), and partially filled by pore-filling (Figure 6a-c) and sparitic rim cements (Figure 6e). The elongated pores are observed throughout the growth layers which are preferably thin micrite (Figure 7a, c) and the others (Figure 7d). These pores are partially filled by pore-fillings (Figure 7a), dog-tooth (Figure 7b, d) and sparitic rim (Figure 7e) cements as well as internal sediments. The internal sediment consists mainly of micrite as well as silt-sized clastic carbonates (Figure 7f).

5.2. X-RAY DIFFRACTION ANALYSIS

The mineralogical compositions of the powdered subsamples were determined by X-Ray Diffraction (XRD) (Figure 8). Calcite was identified by the diagnostic sharp peaks at 3.03 Å followed by 3.86, 2.84, 2.49, 2.28, 2.09, 1.91, 1.87, and 1.60 Å. A small amount of feldspar was determined by a faint peak at 3.17 Å.

5.3. SEM-EDX ANALYSIS

In the growth layers, sparite is common and consists of euhedral and columnar calcite crystals (Figure 9a-b). In the sparite, intercrystalline pores are common and are often enlarged by dissolution (Figure a-b). Partially dissolved calcite crystals are often observed in sparite (Figure 9c) as well as micrite (Figure 9d). Dissolution transforms relatively large crystals with size from micrite to

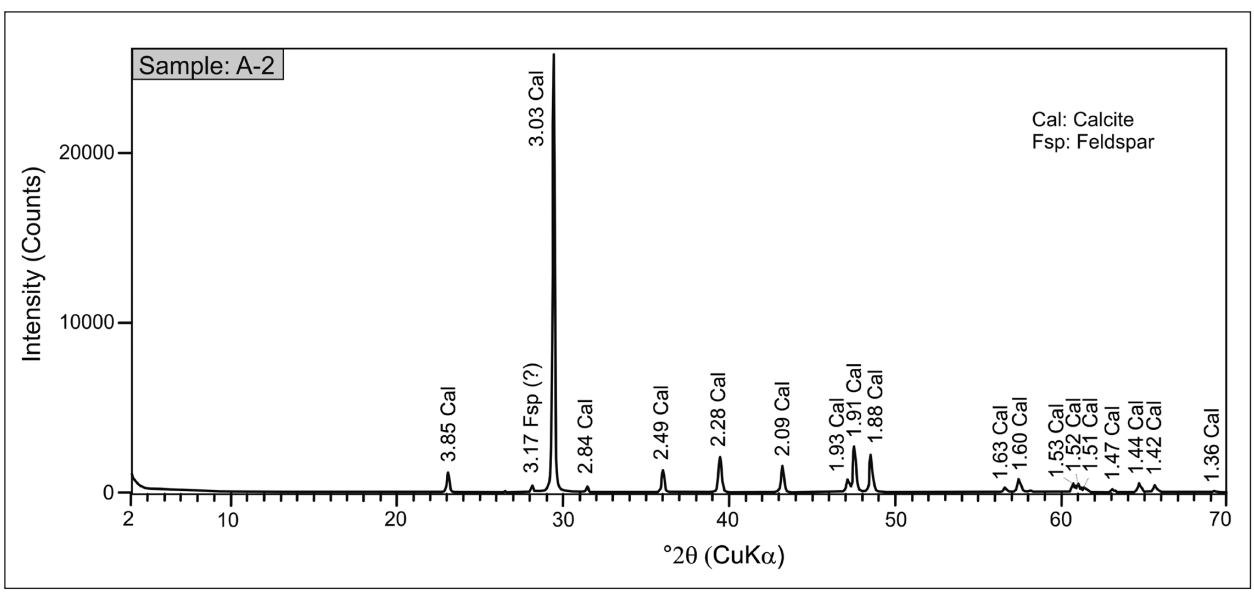

Figure 8: X-ray diffraction pattern of the stalagmite sample showing calcite peaks.

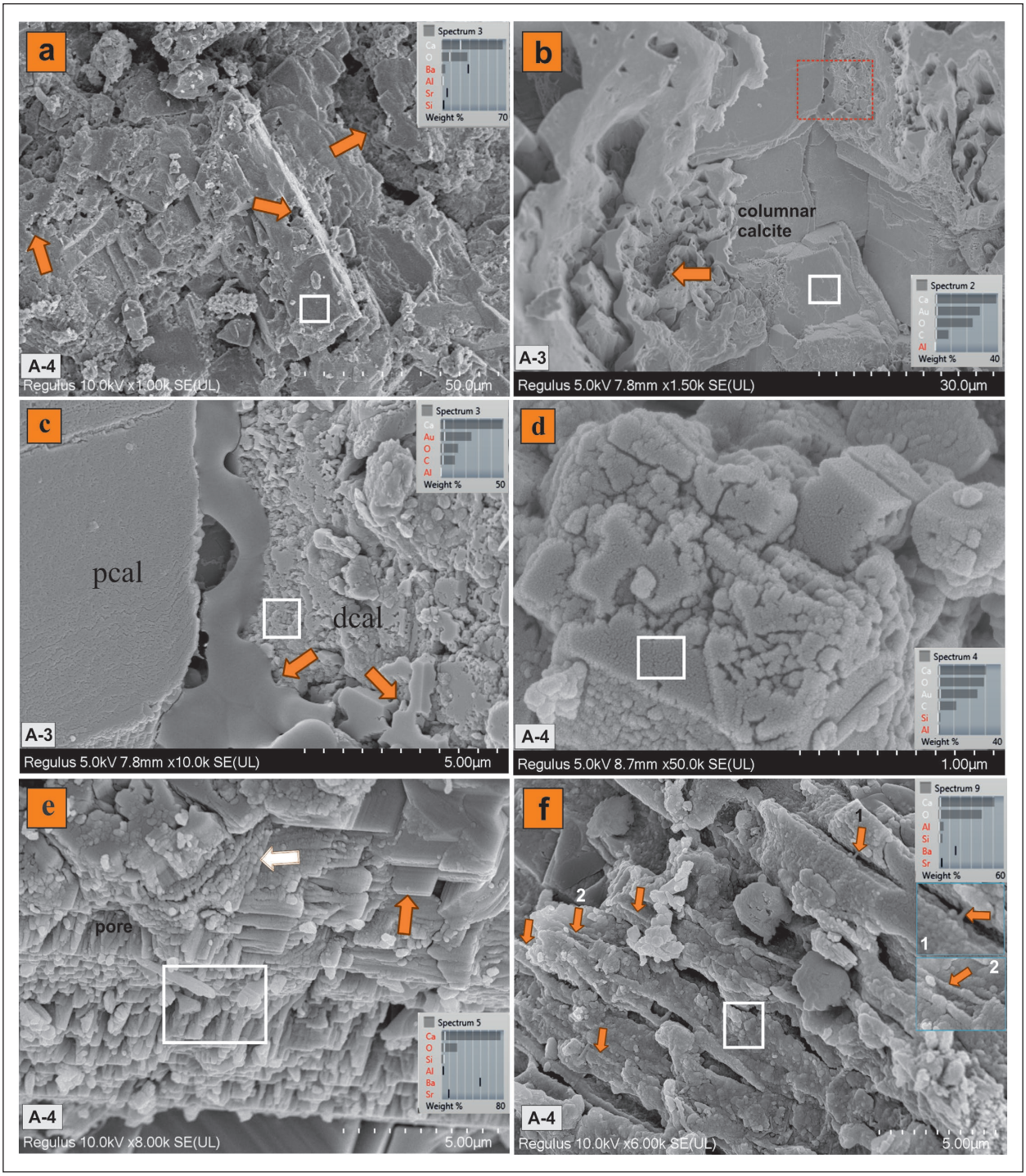

Figure 9: SEM images showing the dissolution characteristics of the stalagmite studied: a) intercrystalline pores enlarged by dissolution (arrows) in microsparite to sparite consisting of euhedral calcite crystals; b) intercrystalline pores enlarged by dissolution (orange arrow) in sparite including columnar-like calcite crystals; c) close up view of the red frame in b) showing preserved (pcal) and partially dissolved (dcal) columnar-like calcite crystals. The partial dissolution of relatively large crystals resulted in the formation of nm-sized crystal aggregates. The arrows indicate dissolutional etching; d) conversion of the relatively large crystals in micrite-size into nm-sized crystal aggregates by dissolution; e) conversion of plate-like calcite (orange arrow) to nm-length crystalline aggregates (white arrow) and pore formation by dissolution on the cleavage surfaces; f) intercrystalline pores enlarged by dissolution between fibrous-like calcite crystals engulfing monocrystalline calcite needles and forming a dendritic fabric. Close-up images of calcite needles at points indicated by arrows 1 and 2 are shown in small blue frames on the right.

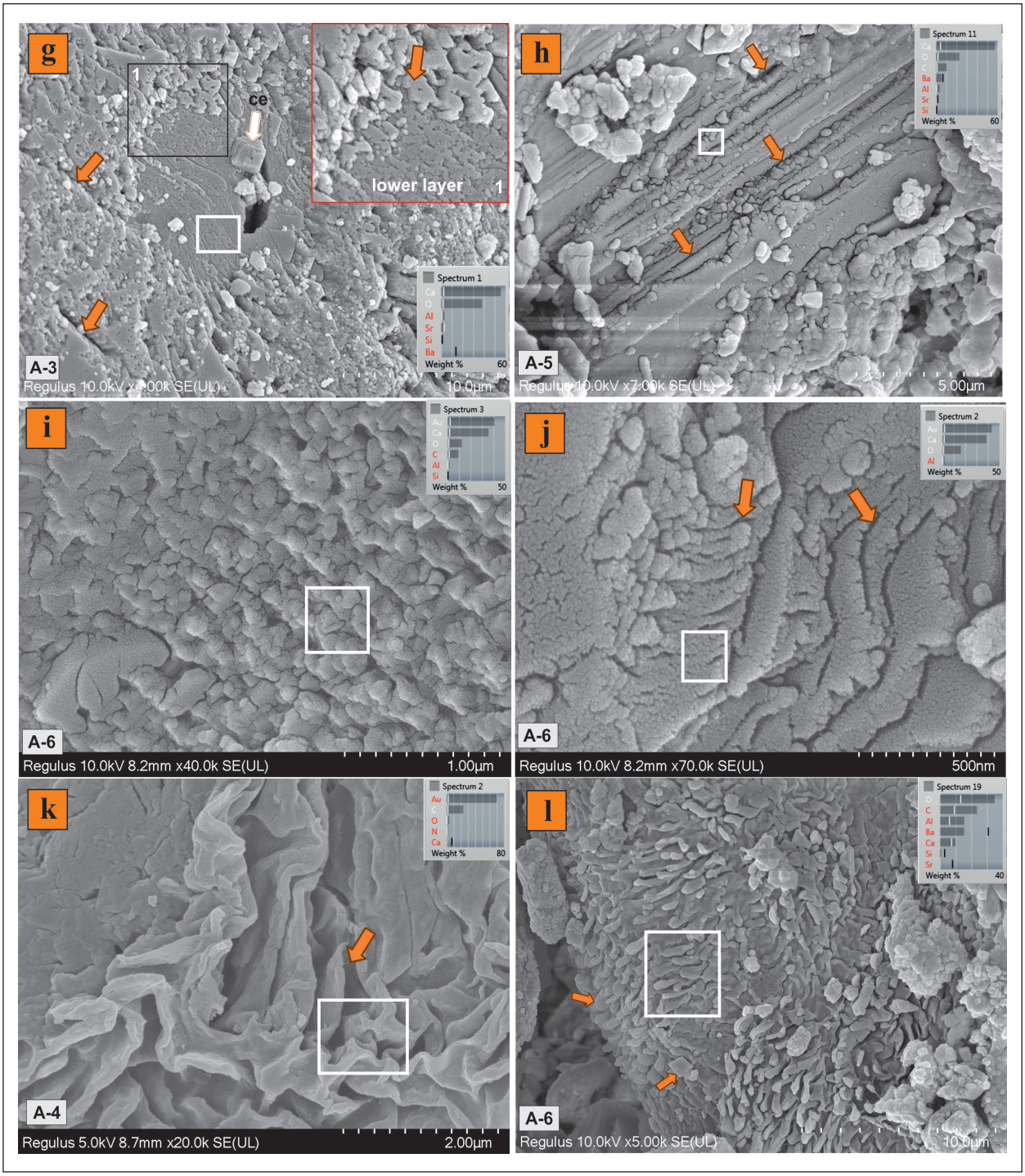

Figure 9: g) a dissolution surface showing the widening and rounding of the crystal boundaries (for detail see close up view of frame 1) and the formation of micro dissolution channels at the crystal boundaries (arrows). The upper micro-layer (arrow) is more affected by dissolution than the lower layer, where the crystal relief is more evident in the enlarged view. ce: calcite cement in pore; h) dissolution along micro-growth layer surfaces or cleavage planes, and consequent formation of elongated pores (arrows) and widened and rounded crystal boundaries; i) growth layer surface showing the influence of dissolution characterized by surface roughness including nano-scale pits, enlarged intercrystalline pores, and crystal boundaries; j) rounded and widened crystal boundaries (arrows); k) widened and rounded crystal boundaries (arrow); l) an image similar to (k) shows the development of these surface structures possibly on plate-like cleavage planes.. The white frames in all images show the area analyzed by EDX and the spectra show the results. Al and Si in (k) and (l) are probably related to clays in surface roughness. Au in the spectra originated from gold coating.

sparite, into small nm-sized crystal aggregates (Figure 9c-d). Dissolution was also affective along the cleavage planes (Figure 9e) and in dendritic fabric that consisting of fibrous-like elongated crystals engulfing the calcite needles (Figure 9f). Dissolution causes the crystal slices to break up into small crystal aggregates and round the edges (Figure 9e, j). Dissolution in the dendritic fabric causes the pores between the fiber-like crystals to enlarge and irregularity at the crystal boundaries, resulting in partial exposure of calcite needles (Figure 9f). In addition, the SEM image shows that the growth layers of the stalagmite are composed of micrite sized calcite crystals interlocking to form a mosaic, and pores exist between the crystals (Figure 9g). Some parts of the growth layers show the intense influence of dissolution (Figure 9g-h) that is characterized by surface roughness including micro-scale dissolution pits (Figure 9g, i), enlarged, rounded crystal boundaries (Figure 9g, j) and strange corrosion surface features (Figure 9k-l). We consider that the strange surface features are enlarged crystal boundaries on the growth layer surface (Figure k) and cleavage surfaces (Figure 9l). In the EDX spectrum of the stalagmite subsamples, the strong Ca peak often associated with faint Si and Al peaks indicates that the subsamples are almost entirely composed of calcite (Figure 9). The EDX spectrum of the unknown surface features given in Figure 9 (k) and (l) differ from the others and are problematic. In Figure 9k, the strong Au peak in the EDX spectra is due to the gold coating on the sample and the increase in its thickness in the solution cavities. This causes the other peaks to be seen at low intensities. A similar situation is created by the clay surface coating (impurity) at another analytical point (Figure 9l).

6. DISCUSSION

Stalagmites are formed by the precipitation of calcite ($CaCO_3$), which forms the growth layers, from a thin film of water under dripping water due to the degassing of CO_2 (Mühlinghaus et al., 2007; Parmentier et al., 2019). The term "micro-karstification" was used here to describe the dissolution process in the stalagmite. The studied stalagmite is composed of calcite based on XRD and SEM-EDX analyses. Dissolution caused widening and rounding of crystal boundaries, the formation of micro-scale pitted and etched crystal surfaces, elongated pores usually parallel to the growth layers (Figure 9), slightly elongated notch-like pores cross-cutting the growth layers (Figure 4b-c) and splitting of relatively larger crystals (≥ micrite) into smaller nanometer-sized crystal aggregates (often ≤ 0.1μm) (Figure 9b-d). The notch-like pores are observed inside the stalagmite subvertically cross-cutting the one or few macroscopic growth layers (Figure 4b-c), and their upper end on the former stalagmite surfaces covered by the newly forming growth layers (Figures 4c; 6a). These pores are more commonly associated with relatively thick sparitic layers showing either often mosaic or columnar calcite fabrics (Figure 6). These observations suggest that dissolution is an early diagenetic event concurrent with stalagmite formation and recurring during stalagmite growth. Their formation is probably due to the enlargement of intercrystalline pores by dissolution in subvertical direction and water seeping into the stalagmite from its former surface (Figures 6; 9a, b, f). These pores allowed water to be transmitted sub-vertically from the top of the stalagmite to the growth layer surface near the surface setting, where water could be transmitted more easily (Figures 4c; 6). Therefore, the former surface morphology of the top of the stalagmite gains importance in this respect since it recently varies from flat to a central depression during this process (Shtober-Zisu et al., 2014). The apex morphology control the residence time of water in the stalagmite which is highly effective for infiltration. The studied stalagmite shows a flat top associated with a small depression without a macro-hole below as mentioned by Shtober-Zisu et al. (2014). We suggest that when the water percolating through the notch-shaped pores reaches the relatively more permeable growth layer, it flows through the surface of this layer towards the stalagmite flank, causing a widespread dissolution within the layer or below its lower surface (Figures 4; 6d; 7). As a result, these dissolved surfaces cause convex/concave breakage along the growth layer surfaces of the stalagmite (Figure 4b-c). Dissolution resulted in micro-scaled pitted crystal surfaces forming surface irregularities (Perrin et al., 2014), enlarged and rounded crystal boundaries and intercrystalline pores, causing weakening of the large calcite crystal fabric and formation of the cryptocrystalline aggregates (called micritization by Neugebauer, 1978; Martín-García et al., 2009; Jones, 2010) on and close to the growth layer surface. In addition, the local calcite rim cement and cement-infill in

the pores indicates repeated dissolution and subsequent partial precipitation processes.

Caves are home to a great variety of chemical reactions in which precipitation/dissolution processes are common and controlled by changes in temperature and/or relative humidity, solution chemistry, pH/Eh, or are mediated by microorganisms (White, 1997). The karst reaction is expressed by the following reaction:

$$CaCO_3 + H_2O + CO_2 \leftrightarrow Ca^{2+} + 2HCO_3^-$$

where, the reaction from left to right consumes carbon dioxide to dissolve limestone, while the reverse reaction causes calcite to precipitate from the water due to the degassing of CO_2 from the water (James & Choquette, 1984; Onac & Forti, 2011). When slightly acidic cave water penetrates into the stalagmite, it partially dissolves the pre-formed carbonates in turn forming different dissolution features (Thamodi & Kumara, 2020). The acidic character of meteoric water is produced naturally when rainwater absorbs CO_2 from the atmosphere and additional CO_2 from the soil in the epikarst zone. During the wet season, probably in times of rainfall greater than normal (Railsback et al., 2013), rapid percolating water may not have enough time to dissolve the host-rocks of limestone in the epikarst zone and may still be undersaturated with respect to the calcite when it reaches the cave. This interpretation is supported by the thin epikarst zone (Figure 3) above the Küpeli cave associated with fractures (Akgöz, 2012). In addition, the cave air and temperature in the first room are highly affected by air conditions out side the cave due to the cave ventilation which was also effective on the precipitation/dissolution processes. The wet period with low temperature has most probably caused an increase in the solubility of the water and in turn the dissolution or corrosion may have occurred in the cave without the effect of precipitation (Kaufmann, 2003; Pagliara et al., 2010; Scholz et al., 2014). The other possibility may be the microbial influence on the dissolution mentioned in some literature (e.g., Pacton et al., 2013; Shtober-Zisu et al., 2014; Johnston et al., 2021) and high cave air CO_2 concentrations (e.g., Kukuljan et al., 2021). The dentritic fabric under the microscope supports the presence of microbials consisting of fiber calcite crystals oriented at different direction. The SEM images reveal that the fiber calcite crystals contain monocrystalline calcite needles which are attributed to fungal origin (Figure 9f; Eren et al., 2021 and other references). At this point, we, thus propose that the microbes provide additional CO_2 to increase the dissolution capability of the cave water on the stalagmite. In addition, the dendritic fabric increases the permeability and consequently water infiltration. In addition, the dendritic fabric increase the permeability that make more easy water infiltration. The pore-rim and pore-filling secondary cements in the pores are probably formed during the dry periods when the interaction time of the leached water in the soil and epikarst zone increases that causes the water to become more saturated with respect to calcite. Cementation in the stalagmite reduces water permeability and infiltration, especially in the notch-shaped pores, and causes a new growth layer to form on the former outer surface of the stalagmite covering the upper end of the notched pores, and consequently ending the dissolution/preprecipitation process within the stalagmite. These processes are controlled by the seasonal fluctuations of the local climate.

In overall, this study suggest dissolution inside the stalagmite concurrent with stalagmite formation or growth, but soon after the formation of one or more growth layers. However, Railsback et al. (2013) stated that dissolution developed at the crest of a stalagmite during the growth, forming chemically truncated or eroded surfaces called E-type layer-bounding surfaces.

CONCLUSIONS

Dissolution features were observed extensively in the studied stalagmite collected from Küpeli Cave in southern Turkey. Dissolution resulted from the cave water percolated along the notch-like sub-vertical pores and subsequently elongated pores parallel to growth layer surfaces. Dissolution preferentially developed along the growth layer surfaces and caused convex or concave breakage of the stalagmite along growth layer surfaces in turn causing the enlargement and roundness of crystal boundaries and intercrystalline pores and micro-scaled pitted crystal surfaces. Finally dissolution caused a breakdown of the large crystals into nm sized crystal aggregates. Repeated dissolution and calcite re-precipitation at different parts of the stalagmite, due to the variation in CO_2 saturation and Ca^{2+} contents of water, mainly in the epikarst zone and also in the stalagmite, are responsible for the formation of the rims and cement infills in pores. Dissolution in the stalagmite most likely occurred during the rainy periods following drier spells.

ACKNOWLEDGEMENT

This article is the updated and improved version of the most prominent stalagmite studied in the second author's master's thesis. The authors are grateful to Andrea Martín Pérez and the anonymous reviewer for their constructive comments and suggestions that improved the quality of the article significantly.

REFERENCES

Aharon, P., Rasbury, M., Murgulet, V., 2006. Caves of Niue Island, South Pacific: Speleothems and water geochemistry. In: Harmon, R.S., Wicks, C. (Eds.), Perspectives on karst geomorphology, hydrology, and geochemistry - A tribute volume to Derek, C., Ford and William B. White. Geological Society of America Special Paper 404, Boulder, pp. 283–295.

Akgöz, M., 2012. Göksu nehri ve Lamas kanyonu (Mersin) arasında kalan bölgenin karst evrimi [PhD Thesis]. Mersin University, 290 pp.

Akgöz, M., Eren, M., 2015. Traces of earthquakes in the caves: Sakarlak Ponor and Kepez Cave, Mersin (S Turkey). Journal of Cave Karst Studies, 77(1): 63–74. http://dx.doi.org/10.4311/2013ES0120

Bar-Matthews, M., Ayalon, A., Kaufman, A., 1997. Late Quaternary palaeoclimate in the eastern Mediterranean region from stable isotope analysis of speleothems at Soreq Cave, Israel. Quaternary Research, 47(2): 155–168.

Domínguez-Villar, D., Wang, X., Cheng, H., Martín-Chivelet, J., Edwards, R.L., 2008. A high-resolution late Holocene speleothem record from Kaite Cave, northern Spain: $\delta^{18}O$ variability and possible causes. Quaternary International, 187(1): 40–51.

Eren, M., 2008. Olba (Ura-Uğuralanı) jeoarkeolojisi (Silifke, Mersin). In: Dönmez, H., Özme, A. (Eds.), 24. Arkeometri Sonuçları Toplantısı, Kültür ve Turizm Bakanlığı Yayın No: 3173, Ankara, 26-30 Mayıs 2008, pp. 181–192 (in Turkish).

Eren, M., Akgöz, M., Kadir, S., Kapur, S., 2021. Primary characteristics of selected stalagmites from four caves located between Erdemli and Silifke (Mersin), southern Turkey—implications on their formation. Carbonates and Evaporites, 36:2. http://doi.org/10.1007/s13146-021-00684-y

Frisia, S., 2019. Stalactites and stalagmites. In: White, W.B., Culver, D.C., Pipan, T. (Eds), Encyclopedia of caves. 3th edition. Academic Press, London, pp. 1041–1048.

Fleitmann, D., Cheng, H., Badertscher, S., Edwards, R.L., Mudelsee, M., Göktürk, O.M., Fankhauser, A., Pickering, R., Raible, C.C., Matter, A., Kramers, J., Tüysüz, O., 2009. Timing and climatic impact of Greenland interstadials recorded in stalagmites from northern Turkey. Geophysical Research Letters, 36(19): L19707. https://doi.org/10.1029/2009GL040050

Gedik, A., Birgili, Ş., Yılmaz, H., Yoldaş, R., 1979. Mut-Ermenek-Silifke yöresinin jeolojisi ve petrol olanakları. Türkiye Jeoloji Kurumu Bülteni, 22:7–26 (in Turkish).

Göktürk, O.M., Fleitmann, D., Badertscher, S., Cheng, H., Edwards, R.L., Fankhauser, A., Tüysüz, O., Kramers, J., 2011. Climate on the southern Black Sea coast during the Holocene: implications from the Sofular Cave record. Quaternary Science Reviews, 30(19-20): 2433–2445. https://doi.org/10.1016/j.quascirev.2011.05.007

James, N.P., Choquette, P.W., 1984. Diagenesis 9. Limestones– The Meteoric diagenetic environment. Geoscience Canada, 11(4): 161–194.

Johnston, V.E., Martín-Pérez, A., Skok, S., Mulec, J., 2021. Microbially-mediated carbonate dissolution and precipitation; towards a protocol for *ex–situ*, cave–analogue cultivation experiments. International Journal of Speleology, 50(2): 137–155. https://doi.org/10.5038/1827-806X.50.2.2372

Jones, B., 2010. Microbes in caves: Agents of calcite corrosion and precipitation. Geological Society London Special Publications, 336(1): 7–30. http://dx.doi.org/10.1144/SP336.2

Kaufmann, G., 2003. Stalagmite growth and palaeo-climate: the numerical perspective. Earth and Planetary Science Letters, 214: 251–266.

Kukuljan, L., Gabrovšek, F., Covington, M.D., Johnston, V.E., 2021. CO2 dynamics and heterogeneity in a cave atmosphere: role of ventilation patterns and airflow pathways. Theoretical and Applied Climatology, 146: 91–109. https://doi.org/10.1007/s00704-021-03722-w

Martín-García, R., Alonso-Zarza, A.M., Martín-Pérez, A., 2009. Loss of primary texture and geochemical signatures in speleothems due to diagenesis: Evi-

dences from Castañar Cave, Spain. Sedimentary Geology, 221(1): 141–149. http://dx.doi.org/10.1016/j.sedgeo.2009.09.007

Mühlinghaus, C., Scholz, D., Mangini, A., 2007. Modelling stalagmite growth and $d^{13}C$ as a function of drip interval and temperature. Geochimica et Cosmochimica Acta, 71(11): 2780–2790. http://dx.doi.org/10.1016/j.gca.2007.03.018

Neugebauer, J., 1978. Micritization of crinoids by diagenetic dissolution. Sedimentology, 25: 267–283.

Onac, B.P., Forti, P., 2011. Minerogenetic mechanisms occurring in the cave environment: an overview. International Journal of Speleology, 40(2): 79–98. http://dx.doi.org/10.5038/1827-806X.40.2.1

Özgül, N., 1983. Stratigraphy and tectonic evolution of the Central Taurides. In: Tekeli, O., Göncüoğlu, M.C. (Eds.), Proceedings of the International Symposium on the Geology of the Taurus Belt, 26-29 September 1983, Ankara, pp. 77–90.

Pacton, M., Breitenbach, S.F.M., Lechleitner, F.A., Vaks, A., Rollion-Bard, C., Gutareva, O.S., Osintcev, A.V., Vasconcelos, C., 2013. The role of microorganisms in the formation of a stalactite in Botovskaya Cave, Siberia– paleoenvironmental implications. Biogeosciences, 10(9): 6115–6130. https://doi.org/10.5194/bg-10-6115-2013

Pagliara, A., De Waele, J., Forti, P., Galli, E., Rossi, A., 2010. Speleothem and speleogenesis of the hypogenic Santa Barbara Cave System (South-west Sardinia, Italy. Acta Carsologica, 39(3): 551–564.

Parmentier, J., Lejeune, S., Maréchal, M., Bourges, F., Genty, D., Terrapon, V., Maréchal, J.C., Gilet, T., 2019. A drop does not fall in a straight line: a rationale for the width of stalagmites. Proceedings of Royal Society A, 475(2231): 20190556. http://dx.doi.org/10.1098/rspa.2019.0556

Perrin, C., Prestimonaco, L., Servelle, G., Tilhac, R., Maury, M., Cabrol, P., 2014. Aragonite–calcite speleothems: Identifying original and diagenetic features. Journal of Sedimentary Research, 84(4): 245–269. https://doi.org/10.2110/jsr.2014.17

Railsback, L.B., Akers, P.D., Wang, L., Holdridge, G.A., Voarintsoa, N.R., 2013. Layer-bounding surfaces in stalagmites as keys to better paleoclimatological histories and chronologies. International Journal of Speleology, 42(3): 167–180. http://dx.doi.org/10.5038/1827-806X.42.3.1

Rowe, P.J., Mason, J.E., Andrews, J.E., Marca, A.D., Thomas, L., Calsteren, P.V., Jex, C.N., Vonhof, H.B., Al-Omari, S., 2012. Speleothem isotopic evidence of winter rainfall variability in northeast Turkey between 77 and 6 ka. Quaternary Science Reviews, 45: 60–72. https://doi.org/10.1016/j.quascirev.2012.04.013

Scholz, D., Tolzmann, J., Hoffmann, D. L., Jochum, K. P., Spötl, C., Riechelmann, D.F.C., 2014. Diagenesis of speleothems and its effect on the accuracy of $^{230}Th/U$-ages. *Chemical Geology*, **387:** 74–86. http://dx.doi.org/10.1016/j.chemgeo.2014.08.005

Shtober-Zisu N., Schwarcz H.P., Chow T., Omelon C.R., Southam, G., 2014. Caves in caves: evolution of post-depositional macroholes in stalagmites. International Journal of Speleology, 43(3): 323–334. http://dx.doi.org/10.5038/1827-806X.43.3.9

Thamodi, A.A.R., Kumara, S., 2020. A geomorphological study on the diversity of micro karst landforms of a limestone cave (with special reference to Waulpane Cave in Ratnapura District). International Journal of Recent Scientific Research, 11: 38831–38842. https://doi.org/10.24327/IJRSR

Turkish State Meteorological Service (DMI), 2020. Unpublished Climatic Data from 1980 to 2019, Erdemli/ Mersin 17958 Station.

Ünal-İmer, E., Shulmeister, J., Zhao, J., Uysal, I.T., Feng, Y., Nguyen, A.D., Yüce, G., 2015. An 80 kyr-long continuous speleothem record from Dim Cave, SW Turkey with paleoclimatic implications for the Eastern Mediterranean. Nature Scientific Reports, 5: 13560. https://doi.org/10.1038/srep13560

Ünal-İmer, E., Shulmeister, J., Zhao, J., Uysal, I.T., Feng, Y., 2016. High-resolution trace element and stable/radiogenic isotope profiles of late Pleistocene to Holocene speleothems from Dim Cave, SW Turkey. Palaeogeography, Palaeoclimatology, Palaeoecology, 452(2): 68–79. http://dx.doi.org/10.1016/j.palaeo.2016.04.015

Vaks, A., Bar-Matthews, M., Ayalon, A., Schilman, B., Gilmour, M., Hawkesworth, C.J., Frumkin, A., Kaufman, A., Matthews, A., 2003. Paleoclimate reconstruction based on the timing of speleothem growth and oxygen and carbon isotope composition in a cave located in the rain shadow in Israel. Quaternary Research, 59: 182–193.

Verheyden, S., Nader, F.H., Cheng, H.J., Edwards, L.R., Swennen, R., 2008. Paleoclimate reconstruction in the Levant region from the geochemistry of a Holocene stalagmite from the Jeita cave, Lebanon. Quaternary Research, 70(3): 368–381. https://doi.org/10.1016/j.yqres.2008.05.004

White, W.B., 1997. Thermodynamic equilibrium, kinetics, activation barriers, and reaction mechanisms for chemical reactions in karst terrains. Environmental Geology, 30(1-2): 46–58.